Hindawi
International Journal of Energy Research
Volume 2023, Article ID 2339117, 14 pages
https://doi.org/10.1155/2023/2339117

Research Article

Detailed Study of Sulfur Poisoning and Recovery of Ni-YSZ-Based Anodes Operating up to 1.8 W cm^{-2} in a Biogas Fuel

Jianjun Ma,[1,2] **Yao Jiang**,[1] **Paul A. Connor**,[2] **Stephen R. Gamble**,[2] **Mark Cassidy**,[2] **Cairong Jiang**,[1,2] **and John T. S. Irvine**[2]

[1]*School of Materials Science and Engineering, Sichuan University of Science and Engineering, Zigong, Sichuan 643000, China*
[2]*School of Chemistry, University of St Andrews, The Purdie Building, St Andrews, Fife, UK KY16 9ST*

Correspondence should be addressed to Cairong Jiang; crjiang@suse.edu.cn and John T. S. Irvine; jtsi@st-andrews.ac.uk

Received 27 September 2022; Revised 14 December 2022; Accepted 26 December 2022; Published 16 February 2023

Academic Editor: Prakash Bhuyar

Ni-YSZ (nickel-yttrium-stabilized zirconia) is a common anode for solid oxide fuel cells (SOFCs) because of its excellent catalytic performance and electronic conductivity. It shows that the nickel anode-supported cell exhibits good cell performance in a biogas fuel of 36CH_4-36CO_2-20H_2O-4H_2-4CO. Unfortunately, natural biogas fuels often contain sulfur, so using nickel anodes is not always straightforward. This paper investigates the sulfur poisoning and the recovery of $BaCe_{0.7}Zr_{0.1}Y_{0.1}Yb_{0.1}O_{3-\delta}$- (BCZYYb-) (Ce, Y, and Yb codoped barium zirconate) impregnated nickel anode-supported cells operating up to 1.8 W cm^{-2} in the biogas. The in situ gas analysis reveals that the suppression of the reforming reactions might cause sulfur poisoning in a 4 ppm (v) H_2S (hydrogen sulfide) in open circuit conditions, whereas the current degradation in working conditions could be attributed to the deactivation of reforming reactions and catalyst activity. The incidence of water-gas shift reactions is associated with the degradation rate of these two reactions. After removing the H_2S, the recovery is accelerated by a steam hydrogen fuel, indicating that steam facilitates the efficient release of sulfur from nickel sites.

1. Introduction

A solid oxide fuel cell (SOFC) attracts more attention being an energy conversion device due to its fuel flexibility and environmental friendliness [1]. Many types of gas, liquid, and solid biomass can be used as fuel in SOFCs [2]. Some successful cases have been reported on the direct use of butane [3] and methane [4]. As a renewable energy, biomass might be a solution to the global warming effect. The abundant biomass resources, like water primrose [5], rice straw [6], and buffalo grass [7], have been converted into biogas, which might provide enough electricity for the rural area, supposing stacks [8] can be in industrialization [9]. However, the fuel impurities have to be solved before industrial application. Nickel tends to react with the impurities, such as sulfur, chlorine, or silicon, triggering a performance loss [10], subsequent degradation [11], or even deactivation [12] of SOFCs [13]. Although no apparent degradation was found in a single SOFC using biogas fuel, add a trace amount of HCl (4, 8, or 12 ppm (v)) under a galvanostatic test at 850°C [14]. However, the whole stack could break due to the corrosion of the sealant by the chlorine compounds [15]. It is, therefore, required to remove these impurities. A chemical purification method [16] has been applied to remove H_2S [17] and HCl [18], with a significant increase in the methane concentration in biogas from 64.76% to 92.35% [19]. As an impurity, sulfur can cause the deactivation, or even the failure of the nickel electrode, over long-term operation [20]. It is challenging to operate SOFCs in any natural biogas containing sulfur impurities [21]. Sulfur poisoning is controlled by many parameters, e.g., working temperature, impurity concentration, and working time [22]. Some studies have addressed the degradation of SOFCs in sulfur in various conditions, such as in pure hydrogen, hydrocarbon, or a gas mixture [23]. In pure H_2, adsorption/oxidation in the presence of a low concentration of sulfur is the main reason for performance loss [24]. High concentration sulfur leads to irreversible performance degradation.

It is more complicated in a mixture of gases due to the interactions between gases and more chemical and electrochemical reactions than in pure hydrogen [25]. Shiratori et al. [26] added 1 ppm (v) H_2S in a 3 : 2 CH_4/CO_2 mixture. They observed a rapid reduction in the reforming reactions within 2 hours of supplying H_2S to a mixture of biogas with a ratio of 1.5 to 1 ($CH_4 : CO_2$ (25 ml/min)) and N_2 (25 ml/min, respectively). Kuramoto et al. found a slight degradation over 1000 hours of durability test under 1 ppm (v) H_2S, but some particles started to sinter in the diffusion layer [10]. Consequently, the carbon monoxide (CO) yield and the reaction rate drop by about 40% [26]. It indicates that the reforming reactions and electrochemical oxidation with H_2 or CO as the fuel are affected by sulfur chemisorption on the active sites in the triple-phase boundary (TPB). However, the performance loss is not fatal and can be recovered entirely after stopping H_2S.

Hauch et al. [27] demonstrated the influence of 2 ppm (v) H_2S in a gas mixture of $CH_4 : H_2 : H_2O = 3 : 1 : 6$ on cell performance and found that sulfur poisoning under low potential was reversible, even if the cell was exposed to 2 ppm (v) H_2S for 500 hours. Li et al. [28] found that the performance was not recoverable in a mixture of $35H_2$-$46CO$-$16N_2$-$3H_2O$ with 12.5 ppm (v) H_2S. The performance regeneration could be improved by adding 10% H_2O or CO_2 to the above gas mixture. Rasmussen and Hagen [29] investigated the reforming activity of anodes with various amounts of H_2S. They found that a ratio of ($CO+CO_2$) to CH_4 dropped by 90% with a low H_2S concentration, indicating that steam reforming of CH_4 was strongly affected even if there was only a small amount of H_2S. There are usually two stages in sulfur poisoning, a quick voltage drop and a slow degradation [27]. The impedance resistance, cell microstructure, and X-ray diffraction (XRD) patterns were identified to investigate possible mechanisms of sulfur poisoning. These characterization methods are mostly posttests and sometimes cannot represent the actual reactions in poisoning [30]. In situ characterization is strongly recommended to differentiate the chemical and electrochemical reactions regarding sulfur poisoning. Up to date, in situ Fourier transform infrared (FTIR) spectroscopy has been used to evaluate the possible responses in H_2S, but a few reports are on the in situ gas analysis in terms of long-term durability. Rasmussen and Hagen and Chlipala et al. confirmed in the experiments that the cell could operate stably for 24 hours under a maximum concentration of 7 ppm (v) H_2S [29, 31]. Besides sulfur poisoning, carbon deposition is another crucial factor that cannot be ignored when carbon-containing gas is used as fuel for SOFCs. Density functional theory calculation shows that the carbon growth mechanisms at the Ni-YSZ interface depend on the interface structure [32]. In considering the possibility of carbon deposition, the sulfur poisoning mechanisms are more complicated.

Some anode materials, such as doped titanate [33], molybdate [34], $La_{0.75}Sr_{0.25}Cr_{0.5}Mn_{0.5}O_3$ [35], vanadate [36], and copper-based oxide [37], show high tolerance to sulfur. However, the cell performance using nonnickel anodes is not high enough to be applied in the industry compared to those with nickel electrodes. The low catalytic activities of the other anode materials need to be improved, and suitable thin electrolyte membranes must be solved before the materials can be used widely [33]. Some extremely high power output has been achieved in Ni-based fuel cells even at low temperatures [38]. Therefore, nickel remains the most used material for carbon-containing fuels like biogas. In an attempt to use a nickel-based electrode in a sulfur-containing fuel, many ways of modifying the Ni-YSZ (nickel-yttrium-stabilized zirconia) system have been developed [23]. Using ScSZ (Sc-doped zirconia) electrolytes to replace YSZ increased the ability of sulfur tolerance, no fatal voltage drop was observed by adding 100 ppm (v) H_2S to the hydrogen fuel [39]. Coating or infiltration is another effective way of protecting nickel from direct exposure to H_2S [40]. A layer of Nb_2O_5 was coated on the Ni-YSZ surface, resulting in good electrical conductivity, enhanced sulfur resistance, and excellent catalytic activity [41]. Ceria-based materials, such as CeO_2 [42], $Sm_{0.2}Ce_{0.8}O_2$ [43], and $Sm_{0.2}Ce_{0.8}Y_{0.1}Yb_{0.1}O_{1.9}$ [44], were also introduced to Ni-YSZ electrodes exposed to sulfur. Ni-YSZ with infiltrated $Sm_{0.2}Ce_{0.8}O_2$ operated more stably in H_2 containing 60 ppm (v) H_2S fuel than without $Sm_{0.2}Ce_{0.8}O_2$. The cell did not fail at a high H_2S concentration, up to 500 ppm (v) [43]. Recently, barium zirconate-based anode [45] and BaO [46] were reported to have an excellent ability to resist carbon coking and sulfur poisoning.

Previous research showed that Ni-YSZ exhibited a good cell performance operating in biogas composed of $36CH_4$-$36CO_2$-$20H_2O$-$4H_2$-$4CO$, especially infiltrated with $BaZr_{0.1}Ce_{0.7}Y_{0.1}Yb_{0.1}O_{3-\delta}$ (BCZYYb) [47]. We aim to investigate the sulfur poisoning and the recovery of a bare nickel-based cell and the cells impregnated with BCZYYb operating up to 1.8 W cm^{-2} in a biogas fuel of $36CH_4$-$36CO_2$-$20H_2O$-$4H_2$-$4CO$ both in operational conditions and in equilibrium states by in situ gas analysis.

2. Experimental

2.1. Single-Cell Preparation. The cell used in the experiment was homemade in this study. Details of the preparation process and BCZYYb-based cells have been described in our previous papers [2, 47]. The cell was impregnated with BCZYYb 3 times, 6 times, and 9 times to obtain different amounts of proton conductors. Correspondingly, the proton content was 0.6 wt%, 1.0 wt%, and 1.6 wt% based on the total weight of each cell. The cell was defined as Ni-YSZ-3BCZYYb, Ni-YSZ-6BCZYYb, and Ni-YSZ-9BCZYYb. The impregnated BCZYYb and the $(La_{0.8}Sr_{0.2})_{0.95}MnO_3$-YSZ (LSM-YSZ) cathode were thermal-treated at 1100°C for two hours. Finally, the current collector for the cathode and anode was Pt and Au paste, respectively.

2.2. Electrochemical Test. The cell (sealed with Aremco 552 sealant) was heated to 800°C with a thermocouple to detect the temperature, remaining at 100°C and 250°C for one hour to obtain good sealing. Argon gas was purged to protect the cell from being oxidized. Hydrogen gas started to supply when the target temperature was reached. The cathode was supplied with flowing air. The open circuit voltage (OCV)

was monitored to reach an equilibrium state before testing. Initially, cell performance at 800°C was characterized by linear sweeps and electrochemical impedance spectra on Solartron 1280B (UK). The electrochemical impedance spectra (EIS) were collected in open circuit conditions.

After the open circuit voltage (OCV) reached a constant value, the anode gas bubbled through the water to get humidified hydrogen. The I-V-P (current-voltage-power density) curves and EIS of the cell were tested in humidified H_2 (3%H_2O). And then, 20% steam was applied by a steam generator. The cell performance was tested under 20%H_2O-H_2. Afterward, a biogas mixture of 36% CH_4, 4% H_2, 4% CO, 36% CO_2, and 20% H_2O balanced with 15 ml min^{-1} argon reference gas to obtain a 300 ml min^{-1} in total was fed to the anode. There was 5% argon in the feed gas. The volume of outlet gases might increase after reforming and electrochemical reactions. Therefore, the percentage of argon would further decrease. The cell performance was tested again. A 4 ppm (v) H_2S was then added (using 100 ppm (v) in hydrogen, 4% hydrogen in the total stream) for the next 24 hours. The OCV was first monitored for 2 hours, and the gases from the outlet of the anode chamber were also detected. After that, the current of cells was recorded, while a 0.7 V voltage load was added to the cell for the next 22 hours. The sulfur was removed, and the EIS and the I-V-P curves were measured again. The recovery of the current density in the biogas for 20 hours and the 20% steam hydrogen for 24 hours was carried out at 0.7 V.

2.3. Gas Characterization. A gas chromatograph (GC, HP 6890, Japan) was used for the in situ measurement of the tailor gas in this study. The gas detection was carried out continuously during the test process operating under open circuit conditions or a load. A reference gas, argon, was added to aid the measurement of the amount of hydrogen gas, as the detection by the GC may not have been accurate enough from the experimental test in our previous paper. More details about the gas analysis were shown in our previous paper [47]. Gases like methane, carbon monoxide, carbon dioxide, and hydrogen were detected by the GC, while the water content (before the trap) was tested using a dew-point sensor (Vaisala, HMT330). The microstructure of the anodes was analyzed using a field emission scanning electron microscope (JEOL JSM-6700, Japan).

3. Results and Discussion

3.1. Sulfur Poisoning of the Bare Nickel Electrode. The poisoning of Ni-YSZ exposed to a 4 ppm (v) sulfur-containing biogas is shown in Figure 1. Figure 1(a) presents the open circuit voltage in biogas after the sulfur supply was recorded. There are four regions in the graph. In region I, the cell is stable in the biogas atmosphere without sulfur. Sulfur is added to the biogas in region II. Unlike previous reports that initial exposure to several ppm (v) H_2S resulted in a rapid drop in the voltage [27], the OCV in this study slightly increased for 2 hours after adding H_2S in region II, which could be because of an increase in hydrogen concentration in the feed gas. The uncertainty of measurement data cannot be ignored. The hydrogen content is calibrated, presuming a constant volume of argon in the inlet and outlet.

Another possibility could be that sulfur is oxidized, and the reaction is shown in

$$H_2S + O^{2-} = \frac{1}{2}S_2 + H_2O + 2e^- \quad (1)$$

$$H_2S + 3O^{2-} = SO_2 + H_2O + 6e^- \quad (2)$$

When H_2S is oxidized into S_2 or SO_2, the OCV is given in equations (3) and (4), respectively [36].

$$E = E^0 - \frac{RT}{2F} \ln\left(\frac{P_{S_2}^{1/2} P_{H_2O}}{P_{H_2S} P_{O_2}^{1/2}}\right), \quad (3)$$

$$E = E^0 - \frac{RT}{6F} \ln\left(\frac{P_{SO_2} P_{H_2O}}{P_{H_2S} P_{O_2}^{3/2}}\right). \quad (4)$$

Aguilar et al. also found a quick response after H_2S is introduced into fuel [36]. The current density increased from 400 mA cm^{-2} to 500 mA cm^{-2} at 0.44 V in the first two to three hours and then decreased. Our results are well agreed with their report. The adsorption process of some species (S or S_2) at the nickel catalyst surface enhanced cell performance in 20 ppm (v) H_2S. A low concentration of H_2S in this study is used so that the OCV increases slightly from 1.043 V to 1.047 V.

A quick voltage drop in the next 7 hours in region III is noticed after sulfur had been supplied for 2 hours. The addition of sulfur brings about a rapid voltage drop, which could be caused by sulfur adsorption. The corresponding result is the prevention of methane conversion (Figure 1(b)). We also see an increase in polarization resistance (Figure 1(c)). Nickel sulfide is not thermodynamically favored under the investigated conditions [48]. Slow degradation of cell OCV was then observed over the next 15 hours in region IV. No stable cell voltage was achieved during the whole exposure period in the H_2S.

Figure 1(b) shows the anode exhaust during the test. It was found that the amount of CH_4 in the output stream increases continuously in sulfur, which indicates that the reforming reaction was prevented by exposure to H_2S. This result is similar to the experimental observation of a 90% drop in the ratio of CO/CH_4, CO_2/CH_4, and $(CO+CO_2)/CH_4$ at a 4 ppm (v) H_2S by Rasmussen and Hagen [29]. The gas change was claimed to be caused by the deactivation of steam reforming in sulfur.

Steam reforming is possible.

$$CH_4 + H_2O \longrightarrow CO + 3H_2 \quad (5)$$

Dry reforming could take place as well.

$$CH_4 + CO_2 \longrightarrow 2CO + 2H_2 \quad (6)$$

It is found that CO_2 and H_2O increase over time, which means equations (5) and (6) might be altered. In other

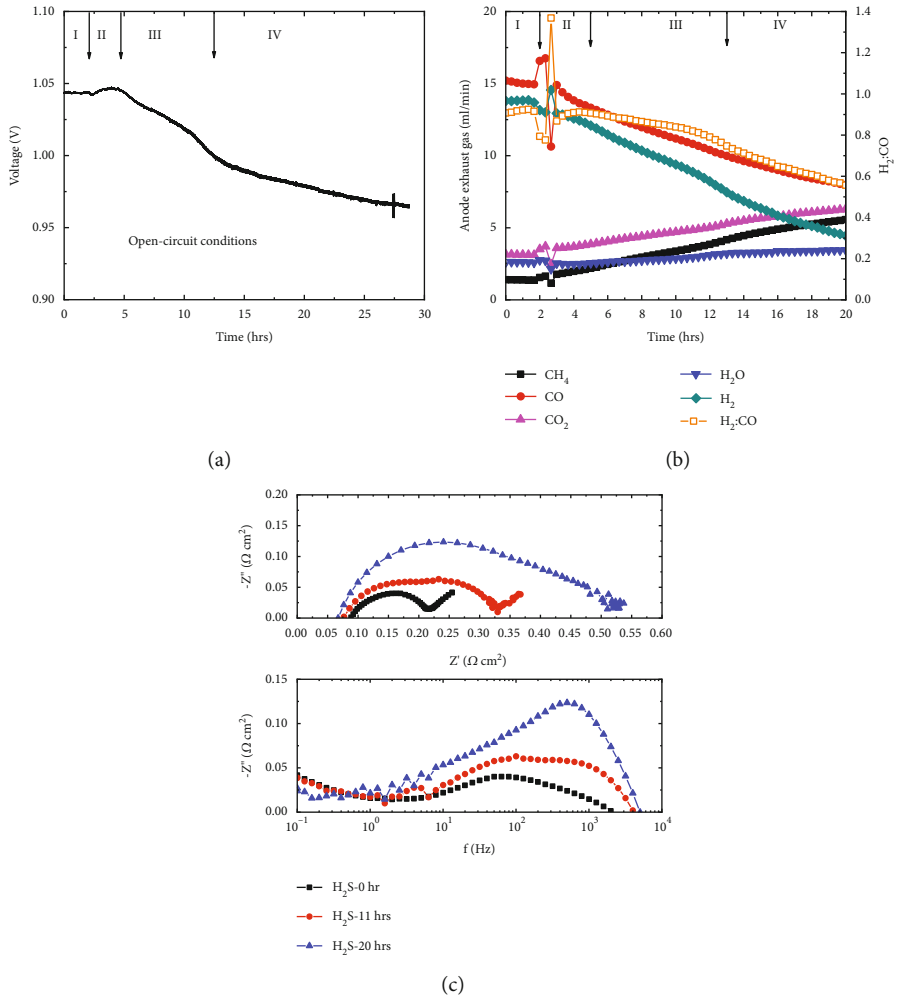

FIGURE 1: Cell performance of the Ni-YSZ on exposure to 4 ppm (v) H_2S. (a) OCV evolution. (b) Anode exhaust gas in open circuit conditions after adding H_2S to the biogas. (c) Impedance spectra patterns in the biogas (black), in the sulfur-containing biogas for 11 hours (red), and in the sulfur-containing biogas for 20 hours (blue).

words, steam and dry reforming are possibly being prevented from exposure to sulfur in open circuit conditions.

Figure 1(c) shows the EIS data for a cell recorded under biogas and after a specific time of exposure to H_2S biogas in open circuit conditions. It is noticed that the ohmic resistance in this study remains constant, and it is even smaller after adding H_2S, which agreed with the report by Li and Wang [49]. They consider that the increased series resistance is attributed to the adsorption of sulfur species (like S or S_2) on the nickel surface. The electrochemical reaction slows down due to less active sites [49]. Our results are not the same as some reports. The polarization and ohmic resistance increased in a $CO/H_2/H_2O$ fuel, even with a low concentration of H_2S [50]. The difference between our results and the report might be caused by the different gas compositions. In the present study, a more complicated system was involved, such as reforming reactions, including steam reforming (as shown in equation (1)) and dry reforming (as shown in equation (2)). These two reactions are involved in the whole process of the cell and are not related to the working conditions. Other reactions like electrochemical reactions and WGS (water-gas shift reaction) should be considered when the cell is working. The polarization resistance is 0.2 Ω cm^2 before sulfur is added, increasing to 0.3 Ω cm^2 exposure to H_2S for 11 hours. The value increases to 0.5 Ω cm^2 after further exposure to the sulfur for 17 hours. Before the exposure to the H_2S, the prevalent resistance was at 100 Hz. After exposure for 11 hours, the dominant resistances were at 1000 Hz and 100 Hz. A significant response to a higher frequency with the addition of H_2S indicates that charge transfer contributes to performance loss, suggesting that the poisoning mechanism could also change [27]. It has been demonstrated that hydrogen oxidation in a hydrogen atmosphere is blocked by sulfur coverage. In a mixture of gases, the poisoning is more complicated.

3.2. Sulfur Poisoning of BCZYYb-Infiltrated Cells. The sulfur poisoning of the cell infiltrated with BCZYYb was investigated in this study as it was reported that BCZYYb has a high tolerance of sulfur (up to 100 ppm (v)) [51]. Previous research demonstrated that an optimal infiltration amount of BCZYYb was 0.6 wt% (Ni-YSZ-3BCZYYb) [47].

Figure 2 shows the performance of the Ni-YSZ-3BCZYYb cell. The power output at 800°C reaches

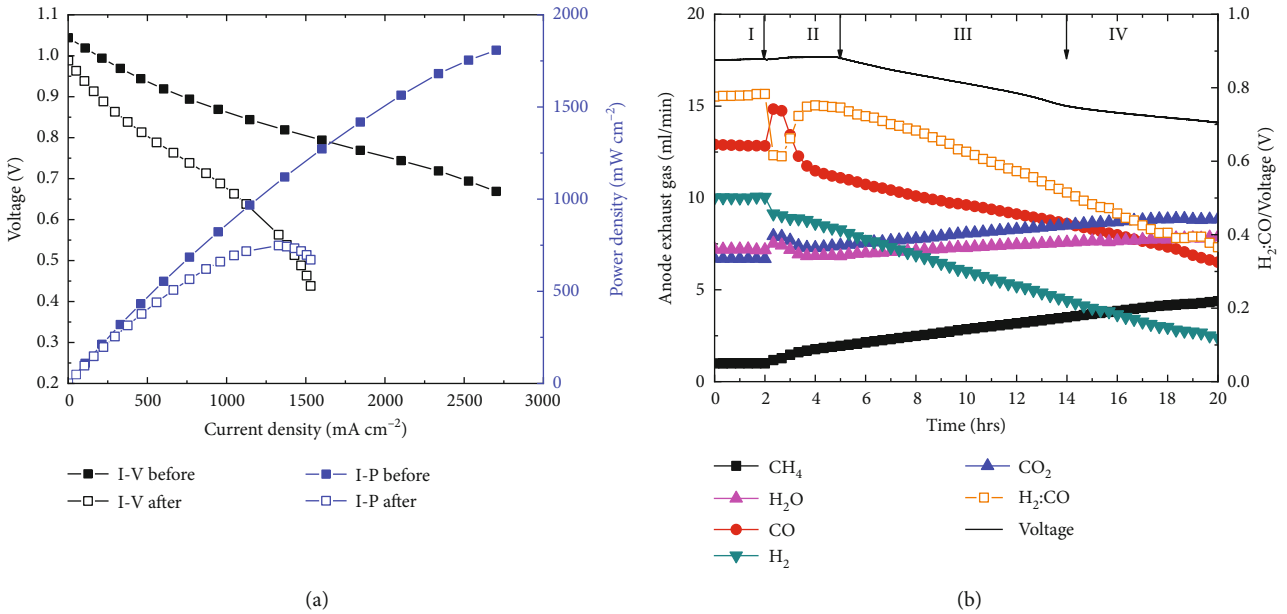

FIGURE 2: (a) Electrochemical performance of the cell Ni-YSZ-3BCZYYb in the biogas operating at 800°C and after poisoning in sulfur for 20 hours. (b) Anode exhaust gases of the cell Ni-YSZ-3BCZYYb in the biogas and the sulfur-containing biogas, considered over a period of time at 1 A cm^{-2}. The changes of the voltage and the ratio of H_2 : CO are also shown.

1.8 W cm^{-2} (Figure 2(a)). As the cell Ni-YSZ-3BCZYYb displays the best performance, the current density at 0.7 V would have been over the current limitation of the testing machine, and the stability was tested at 1 A cm^{-2}. Along with the voltage evolution, the anode exhaust gases are also shown in Figure 2(b). The sulfur poisoning of BCZYYb-impregnated cells is similar to that of the noninfiltrated anodes, and no significant improvement of sulfur tolerance is found in the BCZYYb-infiltrated Ni-YSZ. Blinn and Liu [52] reported that no difference was found between a $BaZr_{0.9}Yb_{0.1}O_{3-\delta}$-modified electrode and a nonmodified one. In region I, the cell voltage gradually increased and reached a stable state at 1 A cm^{-2} current load over a two-hour testing time. After introducing 4 ppm (v) sulfur, the cell voltage steadily increases for about 3 hours in region II. Then, its voltage rapidly drops in region III, followed by a slow degradation in region IV. Even though not much difference was found in the cell voltage changes in the infiltrated Ni-YSZ, the gases have a different change trend than those in the noninfiltrated Ni-YSZ. The gases either increase or decrease over time. The increases in CH_4 concentration during the test time might indicate that the sulfur has influenced the reforming reactions. An increase in CO_2 and H_2O is also noticed, meaning that dry and steam reforming reactions are affected. The hydrogen and carbon monoxide concentration decreases over the test period.

The gas content change might be the result of both the poisoning of the reforming and electrochemical reactions. One of the parameters might be the dominant factor in this process; for example, if the electrochemical reaction dominates, the current density value will be the most important. If the reforming reaction dominates, the content of infiltrated BCZYYb will be critical as the reforming reaction is affected by the presence of BCZYYb proton conductors. Despite the deactivation of reforming reactions, there is still enough hydrogen to maintain a constant current of 1 A. Therefore, in this case, hydrogen decreased over time.

Figures 3(a) and 3(b) show the sulfur poisoning of Ni-YSZ-6BCZYYb and Ni-YSZ-9BCZYYb, respectively. There are four regions in the change of current density when the cell is loaded with 0.7 V (Figures 3(a) and 3(b)). The current density increases in region I steadily, while operating in the biogas atmosphere. The current density in region II increases for the first 2-3 hours of the initial exposure to H_2S. A rapid current drop in region III and a slow current degradation in region IV are observed.

Four regions of change are also noticed in the gases. In region I, the CH_4 content is constant as the equilibrium state of reforming is reached. Under electrochemical conditions, the increase of the water content by hydrogen oxidation promotes the WGS reactions. Therefore, the amount of CO_2 increases. When the current density increases, the H_2 and carbon monoxide decrease, and the carbon dioxide and H_2O increase. The faster drop in the CO as compared to the other gases might suggest that the CO is involved in the electrochemical reactions. The deactivation of reforming reactions starts after introducing H_2S in region II and therefore brings about a rapid increase in the CO_2 and H_2O. The additional increase in the current density results in a further increase in the content of CO_2 and H_2O. The current density reaches around 2 A cm^{-2} at the end of region II. More H_2 and CO are consumed to maintain the current at this high level, and at the same time, more H_2O and CO_2 are produced due to the increased current density. In region III, the current density drops rapidly, indicating that the electrochemical reaction is affected by sulfur.

Therefore, the content of hydrogen and CO is increased, which might provide evidence that CO is involved in the

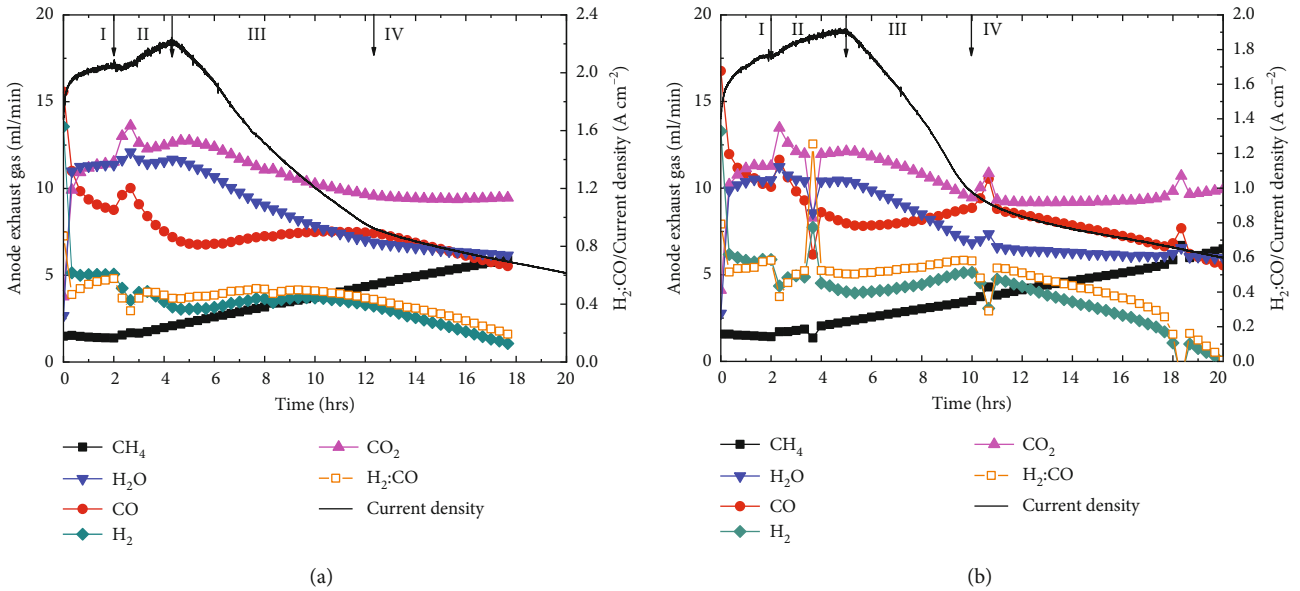

Figure 3: (a) Anode exhaust gases of the cell Ni-YSZ-6BCZYYb in the biogas and in the sulfur-containing biogas, considered over a period of time at 0.7 V. (b) Anode exhaust gases of the cell Ni-YSZ-9BCZYYb in the biogas and in the sulfur-containing biogas, considered over a period of time at 0.7 V. The changes in the current density and the ratio of H_2 : CO are also shown.

electrochemical reactions. Alternatively, more CO is produced because of the increased WGS reaction rate. The deviation of the electrochemical reaction causes the increased content of H_2O and CO_2. Once the current density reaches a high value of 1 A cm^{-2}, the condition is similar to Ni-YSZ; the current density slowly degrades in region IV. In this region, the slow reforming reactions result in the content reduction of the H_2 and CO.

3.3. Mechanism of Sulfur Poisoning. Table 1 summarises the cells used in these experiments. The schematic diagram of the current density and the gases at 0.7 V is presented in Figure 4. The cell was tested for around 2 hours to reach the equilibrium state in the biogas (region I). The poisoning stage of the cell is divided into three regions, regions II, III, and IV. In the first stage of sulfur poisoning (region II), the cell performance increases after introducing H_2S. H_2S might be used as a fuel, taking part in the reactions shown in equations (1) and (2). Therefore, enhanced performance is found in region II. This process lasts about two hours, whether under a voltage/current load or in open circuit conditions.

In the next 10 hours, the cell shows a significant drop in the OCV in open circuit conditions. In the case of a current/voltage load, the voltage/current drops dramatically in region III. The surface of nickel could be covered by the S with the continuous flow of sulfur. The electrochemical reaction active sites might be covered in this case. Therefore, the reforming reactions slow down due to less participation of nickel catalyst in the reactions. Appari et al. also [53] demonstrated that the drop in CH_4 conversion in a mixture of $12.5CH_4$-$8.4CO_2$-$25.2H_2O$-$53.9N_2$ with a 20 ppm (v) H_2S could be related to the deactivation of nickel catalysts. The possible reaction is shown in

$$\mathrm{Ni} + \mathrm{H_2S(g)} \leftrightarrows \mathrm{Ni - S} + \mathrm{H_2(g)} \quad (7)$$

The degradation rate decreases in region IV and sometimes lasts long. It gradually reaches the "saturation" coverage of S/S_2 on nickel catalysts at a given H_2S concentration.

The chemisorption process is reversible. It takes longer for the cell to recover from the deactivation. The regeneration experiment was carried out in biogas, followed by 20% steamed hydrogen. It can be seen that 50% activity of the catalysts recovers after 10 hours in biogas by removing H_2S. It is possible to fully recover after another 10 hours in 20% steamed hydrogen. These results are well agreed with Ashraf et al.'s report [54]. The catalyst activity loss might be due to the coverage of sulfur species (e.g., S or S_2) on the nickel surface. A high adsorption ability of hydrogen removes the sulfur species and then the catalyst recovers its catalytic activity.

The recovery of the cell in the biogas in region V and steam hydrogen in region VI is recorded after the removal of the hydrogen sulfur. The recovery rate in the steam hydrogen in region VI is much faster than in the biogas in region V. This could be because of the increased hydrogen concentration (80% vs. 4%), leading to faster sulfur desorption. It was shown to be the case in SOFC with internal methane steam reforming by Riegraf et al. [55]. It takes time for the cell to allow the electrochemical reactions to take place in the biogas atmosphere. As far as reforming reactions are concerned, it takes longer to reach equilibrium. However, no reforming reactions occur in the steam hydrogen. Therefore, the dissociative adsorption of different species of sulfur (like S or S_2) on the surface of the electrode is

Table 1: Testing regimes for the various cells and current behaviour.

Sample	Electrode	Testing condition	Region I Biogas	Region II Biogas+H_2S	Region III Biogas+$_2S$	Region IV Biogas+H_2S
Cell A	Ni-YSZ	Open circuit conditions	OCV stable	OCV increases	Rapid OCV drop	Slow OCV drop
Cell B	Ni-YSZ	0.7 V	Current increases	Current increases	Rapid current drop	Slow current drop
Cell C	Ni-YSZ-BCZYYb	1 A	Current increases	Current increases	Rapid current drop	Slow current drop
Cell D	Ni-YSZ-6BCZYYb	0.7 V	Current increases	Current increases	Rapid current drop	Slow current drop
Cell E	Ni-YSZ-9BCZYYb	0.7 V	Current increases	Current increases	Rapid current drop	Slow current drop
Cell A	Ni-YSZ	Open circuit conditions	OCV stable	OCV increases	Rapid OCV drop	Slow OCV drop

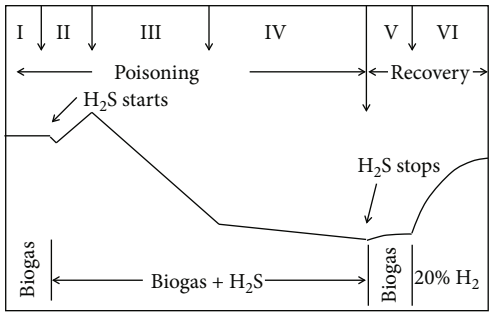

Figure 4: Schematic diagram of the change of current density or voltage on exposure to H_2S.

reasonably fast. The current density almost reverts to its initial value after running in the steam hydrogen for 10 hours. It is also found that the current density continues to increase throughout the testing time (24 hours).

In our previous study, we demonstrated that methane content remains almost at the same level under various current loads, suggesting that methane reforming reactions are not significantly affected by the current load [47]. Figure 5(a) presents the conversion rate of methane during its exposure to H_2S. The best overall conversion rate is obtained with 3BCZYYb-infiltrated Ni-YSZ; however, all the other samples also show a decreasing rate. The inset graph in Figure 5(a) shows the conversion rate of methane in the first few hours. The electrochemical (under current/voltage load) and reforming reactions (in open circuit conditions) are affected. In region I, this rate remains constant in biogas free of sulfur. The methane conversion rate decreases when sulfur is added to the biogas. In region II, the conversion rate begins to change as soon as sulfur is added. At the beginning of the addition of sulfur, 3% less methane is converted through dry reforming and steam reforming, thereby producing a notable increase of CO_2 and H_2O in region II (Figure 4). The variation of the gas components in the anode exhaust leads to a change in the OCV. The OCV decreases to 1.043 V after sulfur is added and then increases to 1.047 V, as shown in Figure 1. Under current/voltage load, the activities of the catalyst deactivate in the presence of sulfur. It suggests that the electrochemical reactions are halted. The drop in CH_4 conversion represents the loss of catalyst activity. The methane conversion rate of the Ni-YSZ-6BCZYYb cell drops from 80% to 22.72% under open circuit conditions in 20 hours. A slightly higher degradation was found on the Ni-YSZ-9BCZYYb cell at 0.7 V from 80% to 9.76%. It suggests that sulfur poisons the reforming reactions. In region III, the open circuit voltage decreases quickly because of the sudden drop in CO and H_2 in the available fuel. In region IV, the open circuit voltage further decreases, but the rate slows down because of the slow poisoning of the reforming reactions.

The electrochemical performance follows the same trend as the open circuit voltage in H_2S. In region I, the current gradually increases in a biogas atmosphere containing no sulfur. The decrease in CO in this region (Figures 1(b), 2(a), 3(a), and 3(b)) would suggest that CO is involved in the electrochemical reactions. The addition of sulfur causes a slight decrease in region II and then increases the current in the following 2-3 hours. This change might result from the gas components by the poisoning of reforming reactions. In region III, the current of the cells decreases dramatically over time, presumably due to the poisoning of the electrochemical reactions.

Faraday's law of electrolysis is shown as [56]

$$n = \frac{\mathrm{It}}{Fv}, \tag{8}$$

where n is the amount of substance with mole as the unit; t is the total time under a given current with s as the unit; I is the current with A as the unit; F is Faraday's constant, 96500 Coulombs/mol; and v is the valency of the ions.

The reversible process of solid oxide electrolysis cells is SOFCs. Therefore, the above equation can be applied to calculate the generated current from fuels in SOFCs. The possible electrochemical reactions in SOFCs are the oxidation of hydrogen or carbon monoxide, as shown in

$$\mathrm{H_2 + O^{2-} = H_2O + 2e^-} \tag{9}$$

$$\mathrm{CO + O^{2-} = CO_2 + 2e^-} \tag{10}$$

Equation (8) can be written as

$$I = \frac{n}{t} Fv, \tag{11}$$

where n/t is the gas flow rate with mole/min as the unit.

Note:

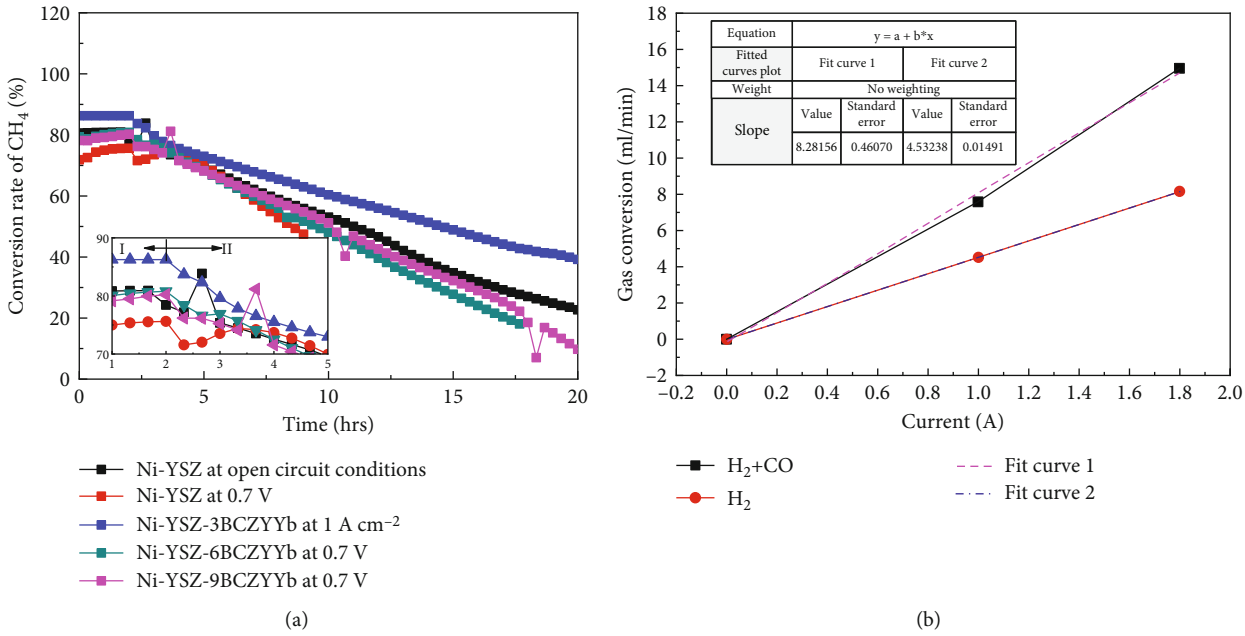

FIGURE 5: (a) CH_4 conversion rate of the cells changes over time in the presence of H_2S. (b) Relation of gas conversion and the current load.

(1) n is the mole of fuels consumed in the whole electrochemical reactions. It includes hydrogen oxidation and electrochemical oxidation of carbon monoxide in this study

(2) υ is the electron involved in the reactions. Here, it is 2 for the reaction of hydrogen oxidation or carbon monoxide oxidation

The volume of fuels consumed in the electrochemical reactions can be obtained by the ideal gas equation [57].

$$\mathrm{PV} = \mathrm{nRT}, \tag{12}$$

where P is the pressure of the tailor gas from the outlet of the anode (KPa), V is the volume of the mixed gas (ml), n is the mole involved in the electrochemical reactions (mole), R is the gas constant (8.314 J/(mol*K)), and T is the temperature of the mixed gas (K).

Combing equations (11) and (12), the current generated by the SOFCs can be expressed with the volume flow rate.

$$I = \frac{n}{t} F\upsilon = \mathrm{QF}\upsilon, \tag{13}$$

where Q is the flow rate of the gases involved in the electrochemical reactions (ml/min).

As long as the gas flow rate is given, the current generation can be obtained using the above equation.

According to equation (13), 7.60 ml/min of fuel is required to produce 1 A current. However, only 4.53 ml/min H_2 is consumed from the gas content (Figure 5(b)). This consumption is obtained from the slope of curve 2 under 1 A current load (Figure 5(b)). Therefore, some other fuels must be taking part in the electrochemical reactions, as shown in equation (10).

According to Figure 5(b), the total consumption of both CO and H_2 of 8.28 ml/min is consistent with the current generation according to equation (13). It suggests that the theoretical production of the current agrees with the electrochemical oxidation of hydrogen and carbon monoxide. In this case, hydrogen could be produced through WGS and then oxidized into H_2O or by the direct oxidation of CO into CO_2. This theoretical value of 8.28 ml/min fitting from curve 1 is slightly higher than the theoretical value of 7.60 ml/min calculated from equation (13), which is 8.8% away from ideal value. The differential could be from the experimental error, which could be improved by repeating the same experimental test on a few samples.

There is no evidence of which path it goes through in the present study. It is reported in the literature that rather than being oxidized directly, CO might be producing hydrogen through WGS, and then, the as-produced hydrogen is oxidation by oxygen ions [50, 58, 59]. The performance loss results from the poisoning of these electrochemical reactions, which is significant at a high current level. It can be seen that CO and H_2 decrease in region III when the current displays a fast degradation (Figure 5(b)). The concentration of H_2O and CO_2 shows the degree of the poisoning of the electrochemical and reforming reactions.

Under open circuit conditions, the level of H_2O and CO_2 increases due to the poisoning of the reforming reactions. Under a constant current, the level of H_2O and CO_2 shows the poisoning of the dry reforming and steam reactions, and at the same time, it remains a constant value to sustain a certain level of current. Therefore, the slope of H_2O and CO_2 under a constant current is consistent with that of the value under open circuit conditions. Under the applied voltage, the actual current values change over time, so the content of H_2O and CO_2 changes over time as well.

When considering the possible poisoning of all kinds of reactions, WGS is an essential reaction involved in mixed gas and has to be considered. It has been shown in the literature that WGS is at the same sites where methane reforming reactions take place. The reaction sites for the above reactions are different from electrochemical hydrogen oxidation sites [59]. We eliminated the influence of the reforming reactions and the electrochemical oxidation by subtracting any methane results in this study since we knew the effect of sulfur on the reforming and electrochemical reactions, as discussed above. Figure 6 shows the four gases of carbon monoxide, water, carbon dioxide, and hydrogen in the anode tailor gas. The corresponding calculated gas components are shown as well in Figure 6. In open circuit conditions, WGS deviates from the equilibrium state and shifts to the reversible WGS (RWGS) direction. WGS is deemed the most favorable reaction, even when added sulfur to hydrogen (Figure 6(a)). It is closest to the equilibrium conditions at the end of the sulfur poisoning test. Under a current load, electrochemical reactions are the priority. WGS is slower than the electrochemical reactions and shifts to the left as the gas components alter in the electrochemical reactions. The initial deviation with the addition of sulfur is insignificant, and it gradually becomes more distinct, indicating that the WGS poisoning in sulfur-containing biogas is getting more severe. In this study, a small anode chamber was used (volume $= \pi \times 1.5^2 \times 30$). Therefore, there was not enough time for all the reactions to reach equilibrium in most conditions. The deviation of WGS might suggest that the electrochemical and reforming reactions do not get their equilibrium state exposed to sulfur. H_2O has to be maintained at a high level by adjusting WGS to sustain a high current of 1 A. It is shown that the electrochemical and chemical reactions are related to the deviation of WGS.

The enhancement of the cell performance with the infiltrated BCZYYb is significant, as shown in the previous paper [47]. After infiltration, there is less CO during the electrochemical process in the presence of H_2S (Figure 6(b)), which might indicate that a proton conductor can act as an accelerator in WGS to some extent. More hydrogen was found in the proton conductor-infiltrated cell than in the noninfiltrated Ni-YSZ cell, which could be because of the enhancement of WGS induced by the presence of the BCZYYb. However, the initial target of enhancing the sulfur tolerance by impregnating the proton conductor of BCZYYb in the Ni-YSZ anode was not achieved. It might also have been due to an insufficient amount of proton conductors being added to the electrode. A maximum of 9BCZYYb was added in this study, presumed to be a small amount not to change the properties of the electrode significantly [45, 51].

3.4. Sulfur Recovery. Figure 7 records the recovery of the Ni-YSZ cell in open circuit conditions after the H_2S was stopped. The open circuit voltage in the biogas had quickly increased from 0.965 V to 1.014 V in 20 hours, indicating that 97% of the open circuit voltage had been recovered within that period after stopping the sulfur supply. The cell performance recovered even faster in the steam hydrogen; the open circuit voltage increased to 1.019 V in 1.6 hours and remained constant during the rest test time. With the removal of the H_2S gas, the OCV started to increase, as shown in Figure 7(a). The recovery rate was slower than the degradation rate in the 4 ppm (v) H_2S. The recovery of cell performance in sulfur-free fuel is a complicated process. If the sulfur poisoning is caused by sulfur adsorption, it needs to desorb after the sulfur removal. The catalyst needs to recover from the reforming and electrochemical reactions. The recovery in the steam hydrogen is much faster than in the biogas. In steamed hydrogen, it is much simpler, as there is only the hydrogen electrochemical reaction to be considered. Other researchers have already examined the function of steam in the recovery of sulfur poisoning [60]. Kim et al. found that in a steam atmosphere, there was a desirable condition for the cell performance to retrieve its original value in a highly concentrated sulfur fuel (5000 ppm (v) sulfur in 50 mol% n-decane) in a Cu-ceria anode [61]. Riegraf et al. found that a high concentration of hydrogen was the accelerator for the recovery from sulfur poisoning [55]. We also found a similar result that cell performance continuously improved in the steam hydrogen throughout the testing period (region VI, Figures 7(b) and 7(c)). Our results confirm that the nickel poisoning induced by sulfur adsorption is removable. It is, therefore, that the cell performance is recoverable. However, the cell voltage did not recover to its initial value, which could also be due to the carbon deposition. It is deemed that both sulfur poisoning and carbon position are the key factors that induce cell performance degradation in a biogas fuel with sulfur impurity. Ni-YSZ interfaces are the preferential position for carbon deposition [32]. In this study, the infiltrated BCZYYb occupies the Ni-YSZ interfaces, making carbon less likely to deposit. The barium-containing proton conductors have excellent water storage ability. These materials also exhibit high ionic and electronic conductivity. The water-gas shift reaction is promoted by the presence of BCZYYb. Therefore, infiltration of BCZYYb suppresses sulfur poisoning and carbon deposition [62]. Our results are in agreement with the report that less carbon deposition is detected at 800°C compared to that at 700°C. In other words, sulfur passivation is a potential strategy to suppress carbon deposition if sulfur poisoning is recoverable.

It has been shown that the recovery can take 24 hours of test time, regardless of the BCZYYb infiltration. In 24 hours, 70% of the cell performance can be recovered. The recovery properties might be related to the potential (or load). The results also indicate that the increase in the infiltration of BCZYYb will shorten the recovery time; for example, the recovery time of the cell Ni-YSZ-6BCZYYb, considered an optimal amount of infiltration, is shorter than that of a noninfiltrated cell. Adsorbed sulfur on an anode surface is quickly released as soon as the H_2S is removed; this happens most rapidly in the initial stages of the recovery process. It is a long distance for the sulfur to transport from the TPB to the anode surface and then be released as the anode is thick (1 mm), especially after a lengthy period of sulfur poisoning. Figure 8 shows the resistance recovery of the cells in the biogas and 20% H_2O-hydrogen. It is found that the cell performance recovers very slowly, and the cell resistance only

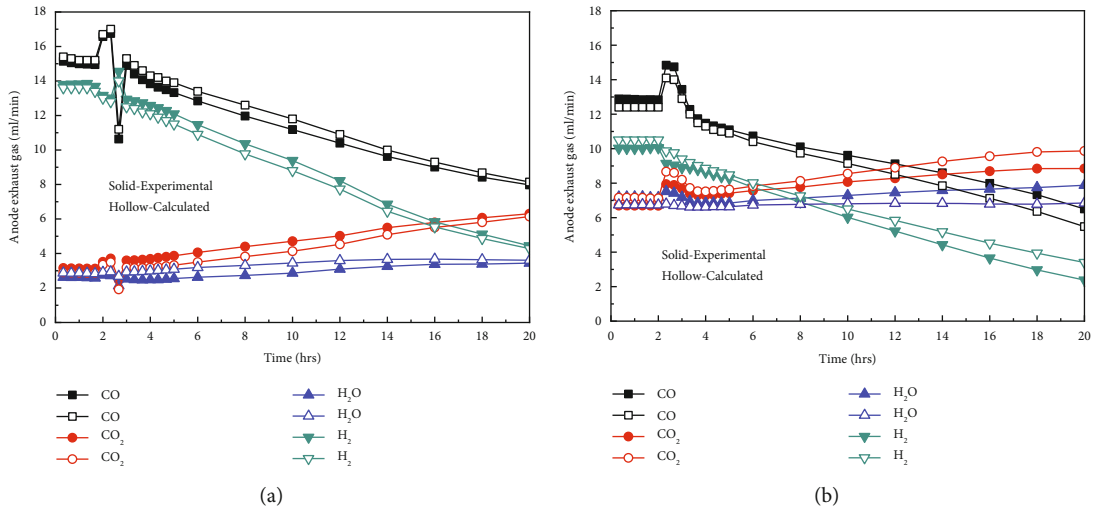

Figure 6: Experimental values of formation rate of four gases of CO, CO_2, H_2O, and H_2 in the anode exhaust gas compared with values expected from equilibrium for this gas input composition. (a) The cell of Ni-YSZ cell in open circuit conditions. (b) The cell 3BCZYYb-NiO-YSZ under 1 A current load.

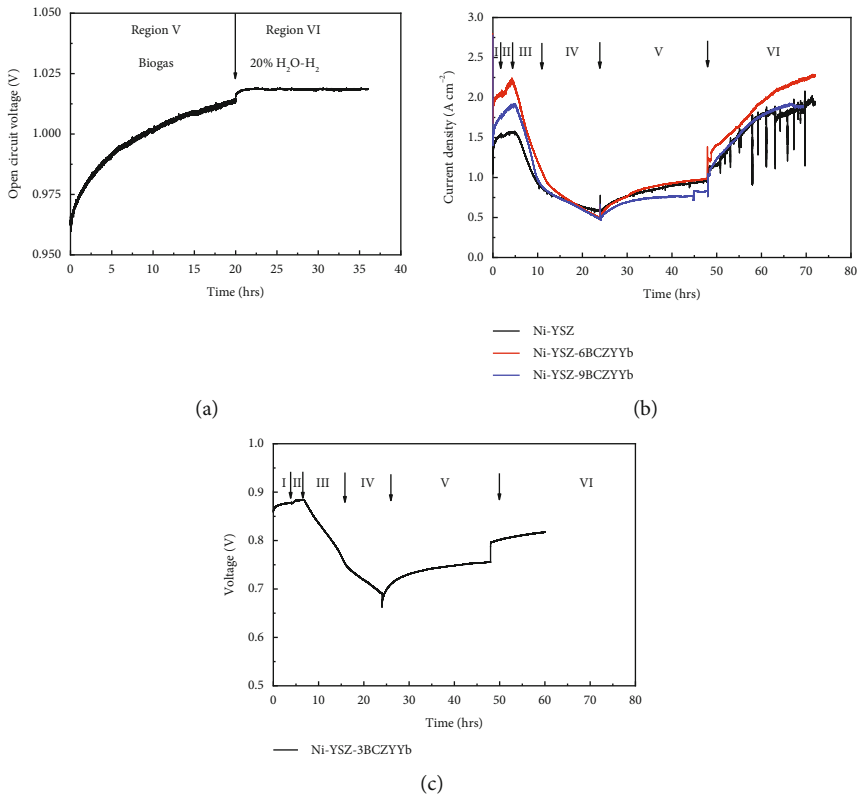

Figure 7: Recovery of cells in different conditions. (a) OCV recovery of the Ni-YSZ cell in the biogas and the steam hydrogen in an open circuit condition after the removal of H_2S. (b) Recovery of the cells in the biogas and steam hydrogen (24 hours in the biogas and the subsequent time was in the steam hydrogen ($20\%H_2O$-H_2)). (c) Recovery of 3BCZYYb/Ni-YSZ in the biogas at 1 A cm^{-2} for 24 hours and in the steam hydrogen at 1 A cm^{-2}.

reduces from 0.65 $\Omega\,cm^2$ to 0.6 $\Omega\,cm^2$ 24 hours after the removal of the sulfur (as shown in Figure 8(a)).

However, the resistance recovered in the steam hydrogen for 24 hours is close to the original value, as is shown in Figure 8(b). It is believed that H_2O is a positive factor for sulfur desorption from the Ni particles when the cell is exposed to sulfur [63].

Figure 9 shows the postimages of the cells in biogas (Figure 9(a)) and biogas with a 4 ppm (v) sulfur (Figure 9(b)). BCZYYb is covered on the surface of grains

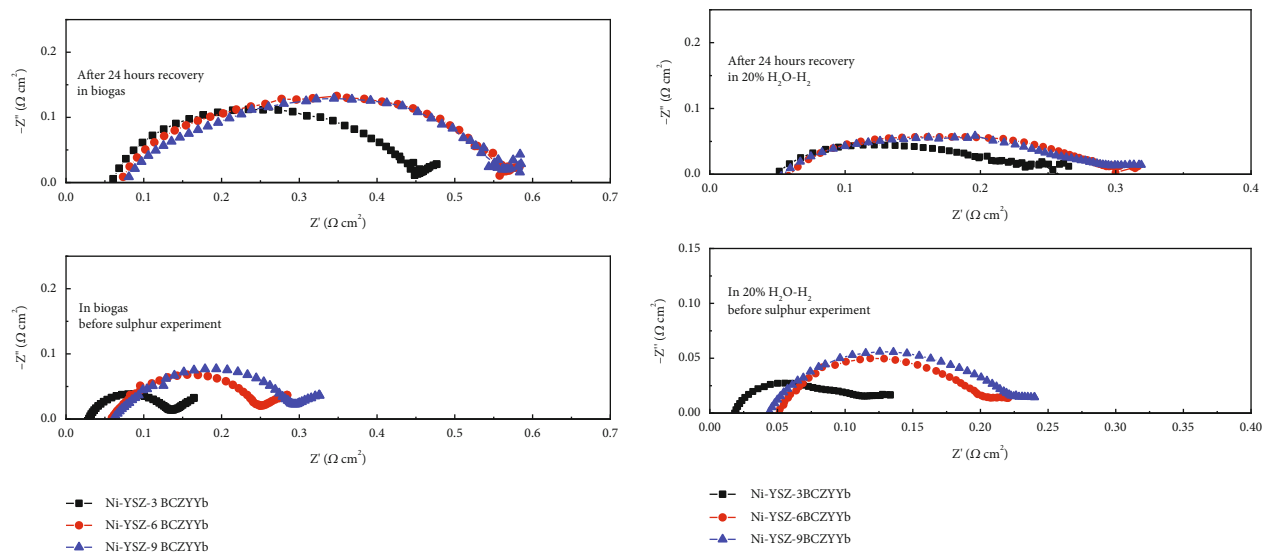

(a) (b)

FIGURE 8: Impedance spectra of the cells. (a) In the biogas before the sulfur experiment and after recovery in biogas for 24 hours. (b) In 20%H_2O-H_2 before the sulfur experiment and after recovery in 20%H_2O-H_2 for 24 hours.

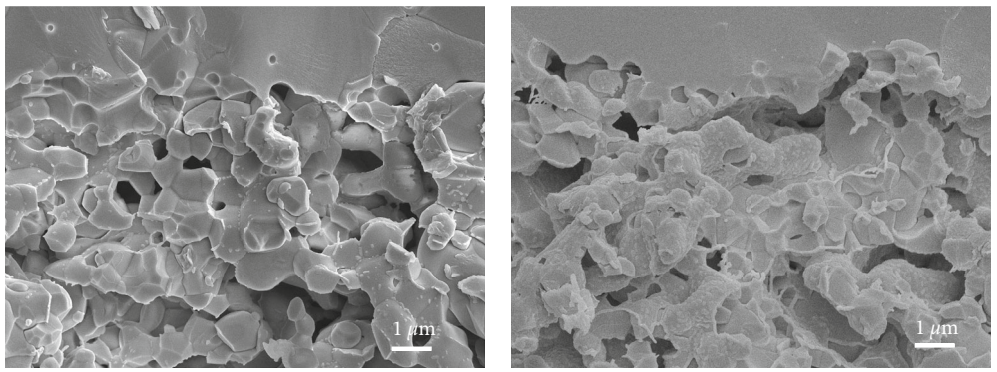

(a) (b)

FIGURE 9: Scanning electron microscopy (SEM) images of the cells. (a) Ni-YSZ-9BCZYYb in biogas. (b) Ni-YSZ-9BCZYYb in biogas with a 4 ppm (v) sulfur.

uniformly. The grains of nickel, BCZYYb, and YSZ are well distributed in the anode. We can see that the anode grains are well integrated with the triple-phase boundary (TPB). It seems that the TPB is not well integrated after the poisoning in the sulfur for 24 hours, even though it has been recovered in steamed hydrogen (Figure 9(b)). There is a more fraction of pore area in the triple-phase boundary. The performance loss is associated with the change in the microstructure, which is proven in Hagen et al.'s report [64]. Further efforts to improve the microstructure of the anode and the triple-phase boundary between the anode and the electrolyte should be made for the cell to be more stable in sulfur.

4. Conclusions

The durability of Ni-YSZ anode-supported cells impregnated with $BaCe_{0.7}Zr_{0.1}Y_{0.1}Yb_{0.1}O_{3-\delta}$ (BCZYYb) operating up to 1.8 W cm^{-2} in sulfur-containing biogas with a composition of 36CH_4-36CO_2-20H_2O-4H_2-4CO was investigated. A 4 ppm (v) H_2S was applied to study the sulfur poisoning in open circuit and electrochemical reaction conditions for around 24 hours. The gas analysis showed that the conversion rate of CH_4 decreased on exposure to sulfur, indicating that sulfur poisoning in the biogas was caused by the reduction of reforming reactions in the equilibrium state. The sulfur poisoning could be seen in three regions: an increase in cell performance in the initial 2-3 hours (region II), a rapid drop of current density in the following 5-7 hours (region III), and slow degradation of current density in 8-10 hours (region IV). H_2O and CO_2 increased due to the quick poisoning of the reforming reactions in region II. A reversible change of all these gases was found in region III. More hydrogen and CO were observed due to the poisoning of electrochemical reactions in H_2S. In region IV, hydrogen and carbon monoxide decreased again, while the amount of H_2O and CO_2 remained unchanged. It suggests that a possible equilibrium state was reached due to the slow

degradation of current density. The impedance spectrum results indicated that the power output loss on the sulfur exposure was owing to increased polarization resistance in the charge transfer process at a high frequency. The recovery experiments in this study showed that the poisoning was reversible despite a 70% performance loss within 22 hours in sulfur. $BaCe_{0.7}Zr_{0.1}Y_{0.1}Yb_{0.1}O_{3-\delta}$- (BCZYYb-) infiltrated Ni-YSZ showed promising electrochemical performance and was highly resistant to sulfur poisoning. However, a small amount of $BaCe_{0.7}Zr_{0.1}Y_{0.1}Yb_{0.1}O_{3-\delta}$ (BCZYYb) was applied, and the sulfur poisoning mechanism needs to be investigated in future research.

Data Availability

Data is available as required.

Conflicts of Interest

The authors declare that they have no conflicts of interest.

Acknowledgments

This research is supported by the EPSRC-DST India-UK project EPI037016/1. This work is also partially supported by the Sichuan Science and Technology Program (under agreement nos. 2021YFH0222 and 2019YFH0177). The authors acknowledge the Zigong Science and Technology Program (under agreement nos. 2020YGJC18 and 2019YYJC24).

References

[1] C. C. Duan, R. J. Kee, H. Y. Zhu et al., "Highly durable, coking and sulfur tolerant, fuel-flexible protonic ceramic fuel cells," *Nature*, vol. 557, no. 7704, pp. 217–222, 2018.

[2] C. R. Jiang, J. J. Ma, A. D. Bonaccorso, and J. T. S. Irvine, "Demonstration of high power, direct conversion of waste-derived carbon in a hybrid direct carbon fuel cell," *Energy & Environmental Science*, vol. 5, no. 5, pp. 6973–6980, 2012.

[3] Y. Wang, L. Sun, L. Luo, Y. Wu, L. Liu, and J. Shi, "The study of portable direct-flame solid oxide fuel cell (DF-SOFC) stack with butane fuel," *Journal of Fuel Chemistry and Technology*, vol. 42, no. 9, pp. 1135–1139, 2014.

[4] S. A. Venancio, P. Emilio, and V. de Miranda, "Direct utilization of carbonaceous fuels in multifunctional SOFC anodes for the electrosynthesis of chemicals or the generation of electricity," *International Journal of Hydrogen Energy*, vol. 42, no. 19, pp. 13927–13938, 2017.

[5] H. T. T. Nong, K. Whangchai, Y. Unpaprom, C. Thararux, and R. Ramaraj, "Development of sustainable approaches for converting the agro-weeds Ludwigia hyssopifolia to biogas production," *Biomass Conversion and Biorefinery*, vol. 12, no. 3, pp. 793–801, 2022.

[6] K. Jiraporn, R. Rameshprabu, K. Sirichai, and D. Natthawud, "Assessment of the biogas potential from agricultural waste in northern Thailand," *Maejo International Journal of Energy and Environmental Communication*, vol. 1, no. 1, pp. 40–47, 2021.

[7] A. Chuanchai and R. Ramaraj, "Sustainability assessment of biogas production from buffalo grass and dung: biogas purification and bio-fertilizer," *3 Biotech*, vol. 8, no. 3, p. 151, 2018.

[8] V. Somano, D. Ferrero, M. Santarelli, and D. Papurello, "CFD model for tubular SOFC directly fed by biomass," *International Journal of Hydrogen Energy*, vol. 46, no. 33, pp. 17421–17434, 2021.

[9] N. Kamalimeera and V. Kirubakaran, "Prospects and restraints in biogas fed SOFC for rural energization: a critical review in Indian perspective," *Renewable and Sustainable Energy Reviews*, vol. 143, article 110914, 2021.

[10] K. Kuramoto, S. Hosokai, K. Matsuoka, T. Ishiyama, H. Kishimoto, and K. Yamaji, "Degradation behaviors of SOFC due to chemical interaction between Ni-YSZ anode and trace gaseous impurities in coal syngas," *Fuel Processing Technology*, vol. 160, pp. 8–18, 2017.

[11] P. F. Zhu, Z. Wu, H. Wang et al., "Ni coarsening and performance attenuation prediction of biomass syngas fueled SOFC by combining multi-physics field modeling and artificial neural network," *Applied Energy*, vol. 322, article 119508, 2022.

[12] S. Z. Golkhatmi, M. I. Asghar, and P. D. Lund, "A review on solid oxide fuel cell durability: latest progress, mechanisms, and study tools," *Renewable and Sustainable Energy Reviews*, vol. 161, article 112339, 2022.

[13] Y. Wang, L. Wehrle, A. Banerjee, Y. Shi, and O. Deutschmann, "Analysis of a biogas-fed SOFC CHP system based on multi-scale hierarchical modeling," *Renewable Energy*, vol. 163, pp. 78–87, 2021.

[14] B. Illathukandy, S. A. Saadabadi, P. C. Kuo et al., "Solid oxide fuel cells (SOFCs) fed with biogas containing hydrogen chloride traces: impact on direct internal reforming and electrochemical performance," *Electrochimica Acta*, vol. 433, article 141198, 2022.

[15] D. Papurello, S. Silvestri, and S. Modena, "Biogas trace compounds impact on high-temperature fuel cells short stack performance," *International Journal of Hydrogen Energy*, vol. 46, no. 12, pp. 8792–8801, 2021.

[16] Y. Unpaprom, T. Pimpimol, K. Whangchai, and R. Ramaraj, "Sustainability assessment of water hyacinth with swine dung for biogas production, methane enhancement, and biofertilizer," *Biomass Conversion and Biorefinery*, vol. 11, no. 3, pp. 849–860, 2021.

[17] G. Van Tran, R. Ramaraj, D. Balakrishnan, A. K. Nadda, and Y. Unpaprom, "Simultaneous carbon dioxide reduction and methane generation in biogas for rural household use via anaerobic digestion of wetland grass with cow dung," *Fuel*, vol. 317, article 123487, 2022.

[18] D. Papurello, S. Silvestri, and A. Lanzini, "Biogas cleaning: trace compounds removal with model validation," *Separation and Purification Technology*, vol. 210, pp. 80–92, 2019.

[19] R. Ramaraj, P. Junluthin, N. Dussadee, and Y. Unpaprom, "Potential evaluation of biogas production through the exploitation of naturally growing freshwater macroalgae Spirogyra varians," *Environment, Development and Sustainability*, pp. 1–12, 2022.

[20] L. Yang, Z. Cheng, M. L. Liu, and L. Wilson, "New insights into sulfur poisoning behavior of Ni-YSZ anode from long-term operation of anode-supported SOFCs," *Energy & Environmental Science*, vol. 3, no. 11, pp. 1804–1809, 2010.

[21] D. Papurello, V. Chiodo, S. Maisano, A. Lanzini, and M. Santarelli, "Catalytic stability of a Ni-catalyst towards

biogas reforming in the presence of deactivating trace compounds," *Renewable Energy*, vol. 127, pp. 481–494, 2018.

[22] H. S. Lee, H. M. Lee, J. Y. Park, and H. T. Lim, "Degradation behavior of Ni-YSZ anode-supported solid oxide fuel cell (SOFC) as a function of H_2S concentration," *International Journal of Hydrogen Energy*, vol. 43, no. 49, pp. 22511–22518, 2018.

[23] A. Cho, B. Hwang, and J. W. Han, "Development of Ni-based alloy catalysts to improve the sulfur poisoning resistance of Ni/YSZ anodes in SOFCs," *Catalysis Science & Technology*, vol. 10, no. 14, pp. 4544–4552, 2020.

[24] Y. M. Choi, C. Compson, M. C. Lin, and M. L. Liu, "A mechanistic study of H_2S decomposition on Ni- and Cu- based anode surfaces in a solid oxide fuel cell," *Chemical Physics Letters*, vol. 421, no. 1-3, pp. 179–183, 2006.

[25] A. L. Vincent, J. L. Luo, K. T. Chuang, and A. R. Sanger, "Promotion of activation of CH_4 by H_2S in oxidation of sour gas over sulfur tolerant SOFC anode catalysts," *Applied Catalysis B: Environmental*, vol. 106, no. 1-2, pp. 114–122, 2011.

[26] Y. Shiratori, T. Oshima, and K. Sasaki, "Feasibility of direct-biogas SOFC," *International Journal of Hydrogen Energy*, vol. 33, no. 21, pp. 6316–6321, 2008.

[27] A. Hauch, A. Hagen, J. Hjelm, and T. Ramos, "Sulfur poisoning of SOFC anodes: effect of overpotential on long-term degradation," *Journal of the Electrochemical Society*, vol. 161, no. 6, pp. F734–F743, 2014.

[28] T. S. Li, H. Miao, T. Chen, W. G. Wang, and C. Xu, "Effect of simulated coal-derived gas composition on H[sub 2]S poisoning behavior evaluated using a disaggregation scheme," *Journal of the Electrochemical Society*, vol. 156, no. 12, pp. B1383–B1388, 2009.

[29] J. F. B. Rasmussen and A. Hagen, "The effect of H_2S on the performance of SOFCs using methane containing fuel," *Fuel Cells*, vol. 10, no. 6, pp. 1135–1142, 2010.

[30] W. M. Harris, J. J. Lombardo, G. J. Nelson et al., "Three-dimensional microstructural imaging of sulfur poisoning-induced degradation in a Ni-YSZ anode of solid oxide fuel cells," *Scientific Reports*, vol. 4, no. 1, p. 5246, 2014.

[31] M. Chlipala, P. Blaszczak, S. F. Wang, P. Jasinski, and B. Bochentyn, "In situ study of a composition of outlet gases from biogas fuelled solid oxide fuel cell performed by the Fourier transform infrared spectroscopy," *International Journal of Hydrogen Energy*, vol. 44, no. 26, pp. 13864–13874, 2019.

[32] L. Y. Fan, C. E. Li, P. V. Aravind, W. W. Cai, M. F. Han, and N. Brandon, "Methane reforming in solid oxide fuel cells: challenges and strategies," *Journal of Power Sources*, vol. 538, article 231573, 2022.

[33] B. B. Niu, C. L. Lu, W. D. Yi et al., "*In-situ* growth of nanoparticles-decorated double perovskite electrode materials for symmetrical solid oxide cells," *Applied Catalysis B: Environmental*, vol. 270, article 118842, 2020.

[34] B. B. Niu, F. J. Jin, J. C. Liu et al., "Highly carbon- and sulfur-tolerant $Sr_2TiMoO_{6-\delta}$ double perovskite anode for solid oxide fuel cells," *International Journal of Hydrogen Energy*, vol. 44, no. 36, pp. 20404–20415, 2019.

[35] S. W. Zha, P. Tsang, Z. Cheng, and M. L. Liu, "Electrical properties and sulfur tolerance of $La_{0.75}Sr_{0.25}Cr_{1-x}Mn_xO_3$ under anodic conditions," *Journal of Solid State Chemistry*, vol. 178, no. 6, pp. 1844–1850, 2005.

[36] L. Aguilar, S. W. Zha, Z. Cheng, J. Winnick, and M. L. Liu, "A solid oxide fuel cell operating on hydrogen sulfide (H_2S) and sulfur-containing fuels," *Journal of Power Sources*, vol. 135, no. 1-2, pp. 17–24, 2004.

[37] A. Fuerte, R. X. Valenzuela, M. J. Escudero, and L. Daza, "Study of a SOFC with a bimetallic Cu-Co-ceria anode directly fuelled with simulated biogas mixtures," *International Journal of Hydrogen Energy*, vol. 39, no. 8, pp. 4060–4066, 2014.

[38] J. G. Lee, J. H. Park, and Y. G. Shul, "Tailoring gadolinium-doped ceria-based solid oxide fuel cells to achieve 2 W cm^{-2} at 550 °C," *Nature Communications*, vol. 5, no. 1, pp. 1–10, 2014.

[39] K. Sasaki, K. Susuki, A. Iyoshi et al., "H[sub 2]S poisoning of solid oxide fuel cells," *Journal of the Electrochemical Society*, vol. 153, no. 11, pp. A2023–A2029, 2006.

[40] S. A. Theofanidis, J. A. Z. Pieterse, H. Poelman et al., "Effect of Rh in Ni-based catalysts on sulfur impurities during methane reforming," *Applied Catalysis B: Environmental*, vol. 267, article 118691, 2020.

[41] S. H. Choi, J. H. Wang, Z. Cheng, and M. Liu, "Surface modification of Ni-YSZ using niobium oxide for sulfur-tolerant anodes in solid oxide fuel cells," *Journal of the Electrochemical Society*, vol. 155, no. 5, pp. B449–B454, 2008.

[42] J. W. Yun, S. P. Yoon, J. Han, S. Park, H. S. Kim, and S. W. Nam, "Ceria coatings effect on H[sub 2]S poisoning of Ni/YSZ anodes for solid oxide fuel cells," *Journal of the Electrochemical Society*, vol. 157, no. 12, pp. B1825–B1830, 2010.

[43] J. W. Yun, H. C. Ham, H. S. Kim, S. A. Song, S. W. Nam, and S. P. Yoon, "Effects of the Sm0.2Ce0.8O2-δmodification of a Ni-based anode on the H_2S tolerance for intermediate temperature solid oxide fuel cells," *Journal of the Electrochemical Society*, vol. 160, no. 2, pp. F153–F161, 2013.

[44] X. L. Zhou, J. M. Zhen, L. M. Liu, X. K. Li, N. Q. Zhang, and K. N. Sun, "Enhanced sulfur and carbon coking tolerance of novel co-doped ceria based anode for solid oxide fuel cells," *Journal of Power Sources*, vol. 201, pp. 128–135, 2012.

[45] L. Yang, S. Z. Wang, K. Blinn et al., "Enhanced sulfur and coking tolerance of a mixed ion conductor for SOFCs: $_{BaZr0.1-Ce0.7Y0.2-xYbxO3-\delta}$," *Science*, vol. 326, no. 5949, pp. 126–129, 2009.

[46] L. M. Liu, K. N. Sun, X. L. Zhou, X. K. Li, M. Zhang, and N. Q. Zhang, "Sulfur tolerance improvement of Ni-YSZ anode by alkaline earth metal oxide BaO for solid oxide fuel cells," *Electrochemistry Communications*, vol. 19, pp. 63–66, 2012.

[47] J. Ma, C. Jiang, P. A. Connor, M. Cassidy, and J. T. S. Irvine, "Highly efficient, coking-resistant SOFCs for energy conversion using biogas fuels," *Journal of Materials Chemistry A*, vol. 3, no. 37, pp. 19068–19076, 2015.

[48] E. H. Edwin, H. Karoliussen, and R. Odegard, "H_2S in natural gas fuel reduces mechanical stress in solid oxide fuel cells," *ECS Proceedings Volumes*, vol. 1997, no. 1, pp. 833–843, 1997.

[49] T. S. Li and W. G. Wang, "The mechanism of H[sub 2]S poisoning Ni/YSZ electrode studied by impedance spectroscopy," *Electrochemical and Solid-State Letters*, vol. 14, no. 3, pp. B35–B37, 2011.

[50] A. Kromp, S. Dierickx, A. Leonide, A. Weber, and E. Ivers-Tiffee, "Electrochemical analysis of sulfur-poisoning in anode supported SOFCs fuelled with a model reformate," *Journal of the Electrochemical Society*, vol. 159, no. 5, pp. B597–B601, 2012.

[51] S. Sengodan, M. F. Liu, T. H. Lim, J. Shin, M. L. Liu, and G. Kim, "Enhancing sulfur tolerance of a Ni-YSZ anode through BaZr0.1Ce0.7Y0.1Yb0.1O3−δinfiltration," *Journal of*

the Electrochemical Society, vol. 161, no. 5, pp. F668–F673, 2014.

[52] K. S. Blinn and M. L. Liu, "$BaZr_{0.9}Yb_{0.1}O_{3-\delta}$ -modified bi-electrode supported solid oxide fuel cells with enhanced coking and sulfur tolerance," *Journal of Power Sources*, vol. 243, pp. 24–28, 2013.

[53] S. Appari, V. M. Janardhanan, R. Bauri, S. Jayanti, and O. Deutschmann, "A detailed kinetic model for biogas steam reforming on Ni and catalyst deactivation due to sulfur poisoning," *Applied Catalysis A: General*, vol. 471, pp. 118–125, 2014.

[54] M. Ashrafi, C. Pfeifer, T. Proll, and H. Hofbauer, "Experimental study of model biogas catalytic steam reforming: 2. Impact of sulfur on the deactivation and regeneration of Ni-based catalysts," *Energy & Fuels*, vol. 22, no. 6, pp. 4190–4195, 2008.

[55] M. Riegraf, V. Yurkiv, G. Schiller, R. Costa, A. Latz, and K. A. Friedrich, "The influence of sulfur formation on performance and reforming chemistry of SOFC anodes operating on methane containing fuel," *Journal of the Electrochemical Society*, vol. 162, no. 12, pp. F1324–F1332, 2015.

[56] "Faraday's laws of electrolysis-Wikipedia," 2022, https://en.wikipedia.org/wiki/Faraday%27s_laws_of_electrolysis.

[57] "Ideal gas law-Wikipedia," 2022, https://en.wikipedia.org/wiki/Ideal_gas_law.

[58] H. P. He, A. Wood, D. Steedman, and M. Tilleman, "Sulphur tolerant shift reaction catalysts for nickel-based SOFC anode," *Solid State Ionics*, vol. 179, no. 27-32, pp. 1478–1482, 2008.

[59] A. Hagen, "Sulfur poisoning of the water gas shift reaction on anode supported solid oxide fuel cells," *Journal of the Electrochemical Society*, vol. 160, no. 2, pp. F111–F118, 2013.

[60] M. Flytzani-Stephanopoulos, M. Sakbodin, and Z. Wang, "Regenerative adsorption and removal of H_2S from hot fuel gas streams by rare earth oxides," *Science*, vol. 312, no. 5779, pp. 1508–1510, 2006.

[61] H. Kim, J. M. Vohs, and R. J. Gorte, "Direct oxidation of sulfur-containing fuels in a solid oxide fuel cell," *Chemical Communications*, vol. 22, no. 22, pp. 2334-2335, 2001.

[62] P. Boldrin, E. Ruiz-Trejo, J. Mermelstein, J. M. B. Menendez, T. R. Reina, and N. P. Brandon, "Strategies for carbon and sulfur tolerant solid oxide fuel cell materials, incorporating lessons from heterogeneous catalysis," *Chemical Reviews*, vol. 116, no. 22, pp. 13633–13684, 2016.

[63] J. F. B. Rasmussen and A. Hagen, "The effect of H_2S on the performance of Ni-YSZ anodes in solid oxide fuel cells," *Journal of Power Sources*, vol. 191, no. 2, pp. 534–541, 2009.

[64] A. Hagen, J. F. B. Rasmussen, and K. Thyden, "Durability of solid oxide fuel cells using sulfur containing fuels," *Journal of Power Sources*, vol. 196, no. 17, pp. 7271–7276, 2011.